

Type-II Dirac nodal chain semimetal CrB₄

Xiao-Yao Hou^{1,2}, Ze-Feng Gao^{1,2}, Peng-Jie Guo^{1,2,*}, Jian-Feng Zhang^{3,†} and Zhong-Yi Lu^{1,2,4‡}

1. School of Physics and Beijing Key Laboratory of Opto-electronic Functional Materials & Micro-nano Devices. Renmin University of China, Beijing 100872, China

2. Key Laboratory of Quantum State Construction and Manipulation (Ministry of Education), Renmin University of China, Beijing 100872, China

3. Institute of Physics, Chinese Academy of Sciences, Beijing 100190, China and

4. Hefei National Laboratory, Hefei 230088, China

(Dated: December 6, 2024)

Dirac nodal line semimetals with topologically protected drumhead surface states have attracted intense theoretical and experimental attention over a decade. However, the study of type-II Dirac nodal line semimetals is rare, especially the type-II nodal chain semimetals have not been confirmed by experiment due to the lack of ideal material platform. In this study, based on symmetry analysis and the first-principles electronic structure calculations, we predict that CrB₄ is an ideal type-II Dirac nodal chain semimetal protected by the mirror symmetry. Moreover, there are two nodal rings protected by both space-inversion and time-reversal symmetries in CrB₄. More importantly, in CrB₄ the topologically protected drumhead surface states span the entire Brillouin zone at the Fermi level. On the other hand, the electron-hole compensation and the high mobility of Dirac fermions can result in large magnetoresistance effects in CrB₄ according to the two-band model. Considering the fact that CrB₄ has been synthesized experimentally and the spin-orbit coupling is very weak, CrB₄ provides an ideal material platform for studying the exotic properties of type-II Dirac nodal chain semimetals in experiment.

I. INTRODUCTION

Topological semimetals with symmetry-protected band crossing have attracted intense theoretical and experimental interest due to numerous novel physical properties, such as topologically protected boundary state, chiral anomaly, chiral zero sound, large magnetoresistance effect, topological catalysis[1–6]. According to both the degeneracy and dimension of band crossing, topological semimetals are divided into zero-dimensional Weyl semimetals[7, 8], Dirac semimetals[9–12], triple degenerate semimetals[13–16], sixfold degenerate semimetals[13, 17, 18], eightfold degenerate semimetals[13, 19, 20], one-dimensional nodal-line semimetals[21–23], and two-dimensional nodal surface semimetals[24]. On the other hand, based on whether the zero-dimensional band crossing has strong tilt along a certain direction, zero-dimensional topological semimetals can also be divided into type-I and type-II topological semimetals, such as type-II Weyl[25–27]. In comparison, type-II topological semimetals have unique physical properties different from type-I topological semimetals such as angle-dependent chiral anomaly and topological Lifshitz transitions[25–27].

One-dimensional nodal line semimetals are divided into Dirac and Weyl nodal line semimetals[21–23]. Moreover, multiple nodal lines can also form nodal chain semimetals, hopf-links nodal line semimetals and so on[28, 29]. Naturally, the band crossing on the nodal lines

can contain type-II Dirac and Weyl points, and the corresponding topological semimetals are called type-II Dirac and Weyl nodal line semimetals respectively. Although several type-I nodal line and nodal chain semimetals have been experimentally confirmed[30–32], type-II nodal line semimetals have rarely been experimentally confirmed due to the lack of an ideal material platform. Until recently, ZrSiSe was confirmed as a type-II nodal line semimetal by angle-resolved photoemission spectroscopy (ARPES) measurement[33]. However, type-II nodal chain semimetals have yet not been experimentally confirmed. Therefore, it is very meaningful to predict type-II nodal chain semimetals with distinct properties for the study of their novel physical properties in experiment.

In this study, based on symmetry analysis and the first-principles electronic structure calculations, we predict that CrB₄ is an ideal type-II Dirac nodal chain topological semimetal protected by the mirrors M_z and M_y (1/2, 1/2, 1/2). In addition, there are also two nodal rings protected by both space-inversion (I) and time-reversal (T) symmetries. More importantly, the topologically protected Fermi arcs of CrB₄ at the Fermi level span the entire Brillouin zone. On the other hand, electron-hole compensation and their high mobility can cause CrB₄ to have large magnetoresistance effect. When spin-orbit coupling (SOC) is considered, CrB₄ transforms from type-II nodal chain semimetal to strong topological insulator with Z_2 topological invariant (1,000).

II. METHOD

The structural optimization and electronic structure calculation of CrB₄ were studied in the framework of

* guopengjie@ruc.edu.cn

† zjf@iphy.ac.cn

‡ zlu@ruc.edu.cn

density functional theory (DFT) [34, 35] in the Vienna ab initio simulation package (VASP) [36–38]. The core electrons as well as the interaction between the core and valence electrons were described by using the projector augmented-wave method [39]. The generalized gradient approximation (GGA) of Perdew-Burke-Ernzerhof (PBE)[40] type was treated with exchange-correlation functional, using an energy cut-off of 600 eV for the plane waves. A $14 \times 16 \times 20$ Monkhorst-Pack k mesh was used for the Brillouin zone sampling of the unit cell. The internal atomic positions were fully relaxed until the forces on all atoms were smaller than 0.01 eV/Å. The tight-binding Hamiltonian was constructed by the maximally localized Wannier functions [41–43] and the corresponding topological properties were obtained by using the WannierTools package [44].

III. RESULTS

Chromium tetraboride (CrB_4), originally suggested to have the $Immm$ space group (No. 71) with the $oI10$ unit cell in Pearson notation, was known for excellent adhesive wear resistance due to its high hardness [45]. Afterwards, Niu et al. [46] experimentally confirmed the existence of orthorhombic space group $Pnmm$ (No. 58) CrB_4 with $op10$ unit cell in Pearson notation, which has a lower symmetry than the former. We optimize the experimental structure for CrB_4 with the orthorhombic $Pnmm$ space group. The optimized lattice constants are $a = 4.72$ Å, $b = 5.47$ Å, and $c = 2.85$ Å. Due to 3d-orbital electrons with strong correlation, CrB_4 may have magnetism. We consider different magnetic structures for CrB_4 , all of which are optimized to nonmagnetic state. CrB_4 is thus a paramagnetic material, which is consistent with the experimental results [49]. The crystal structure of CrB_4 is shown in Fig. 1(a-c). From the a direction, CrB_4 is composed of the Cr atomic layer and the B atomic layer, while the B atomic layer is formed by the distorted hexagon of B atoms (Fig. 1(a) and (c)), which results in the low symmetry of CrB_4 . The point group symmetry of CrB_4 is D_{2h} with generator elements C_{2z} , $C_{2x}(1/2, 1/2, 1/2)$ and I . The bulk and surface Brillouin zone (BZ) with the high-symmetry points and lines are shown in Fig. 1(d).

To study the topological properties of CrB_4 , we calculate its electronic band structure along the high-symmetry directions without spin-orbit coupling (SOC), which is shown in Fig. 2(a). From Fig. 2(a), CrB_4 is a semimetal and has only blue and yellow bands crossing the Fermi level. Moreover, there are band crossings around the Fermi level, thus CrB_4 may be topological semimetal protected by crystal symmetry. Symmetry analysis indicates the band crossing points at the Γ -X and Γ -Y axes are protected by the M_z symmetry. Due to the strong tilt along the Γ -X direction, the crossing point is type-II Dirac point. The crossing point on the Γ -Y axis is not tilted along the Γ -Y direction and is therefore

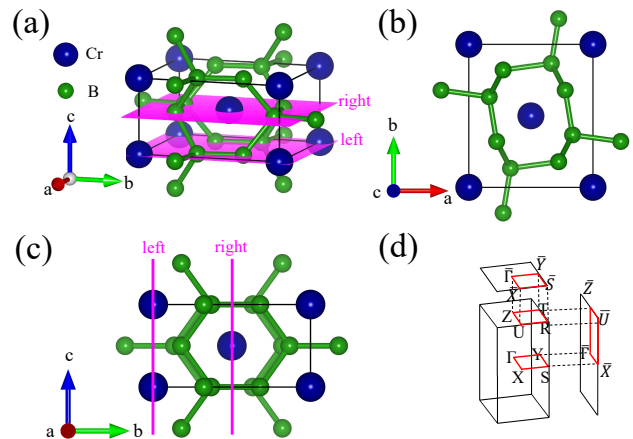


FIG. 1. (a), (b), and (c) are the crystal structures of CrB_4 with side view, top view along the c and a directions, respectively. The magenta planes and lines represent the corresponding left and right terminations. (d) Bulk, (001), and (010) projected 2D surface BZs of CrB_4 , where the high-symmetry lines and the high-symmetry points are marked.

type-I Dirac point. Since the band crossing points on the different directions can lead to a nodal ring, CrB_4 has a nodal ring with both type-I and type-II Dirac points protected by the M_z symmetry. In addition, there is another band crossing in the Γ -X direction protected by $M_y(1/2, 1/2, 1/2)$ symmetry, which is marked by a red arrow. We guess that there may be two small nodal rings in the $k_y=0$ plane protected by the $M_y(1/2, 1/2, 1/2)$ symmetry. To prove our guess, we calculate all the nodes for the blue and yellow bands in the entire BZ, which is shown in Fig. 2(c). As guessed, CrB_4 has indeed two small nodal rings in the $k_y=0$ plane protected by $M_y(1/2, 1/2, 1/2)$ symmetry (Fig. 2(c)). Since the two small nodal rings have a crossing with a larger nodal ring (Fig. 2(c)), CrB_4 is a topological nodal chain semimetal. Besides the nodal chain, there are also two nodal rings located in the non-high-symmetry surface of the BZ, which can be connected by the mirror M_z . The two nodal rings located in the non-high-symmetry surface of BZ are only protected by the IT symmetry (the T represents the time-reversal symmetry and I represents the space-reversal symmetry). In order to show the nodal ring of CrB_4 more directly, we also calculate the three-dimensional diagram of the yellow and blue bands. From Fig. 2(b), the nodal ring in the $M_z=0$ plane has relatively large dispersion and the type-I Dirac points below the Fermi level are clearly shown, which is conducive to observation by the ARPES experiment. Therefore, CrB_4 is an ideal Dirac nodal chain topological semimetal.

Then, we also calculate the three-dimensional Fermi surface of the CrB_4 , which is shown in Fig. 2(d). From Fig. 2(d), CrB_4 has a hole-type Fermi surface (blue) and an electron-type Fermi surface (yellow). Moreover, our calculations show that the volume of the hole Fermi surface is equal to that of the electron Fermi surface,

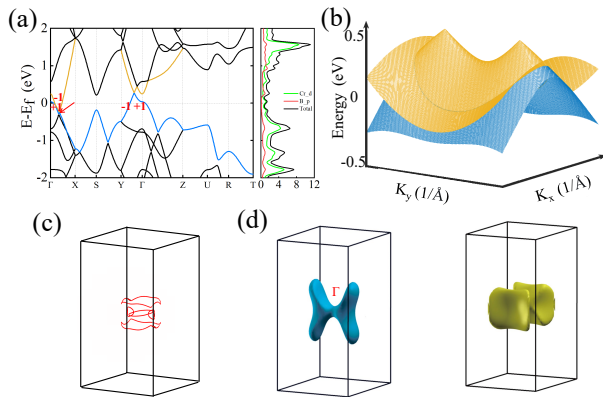


FIG. 2. (a) The band structure along high-symmetry directions(left panel) and density of states (right panel) for CrB_4 without SOC. The +1 and -1 are the eigenvalues of the mirror M_z . (b). Bulk energy dispersions of highest valence (bule) and lowest conduction (yellow) bands in the $k_z=0$ plane. (c) The nodal rings and chain in the BZ for CrB_4 . (d) The hole-type (left panel) and electron-type (right panel) Fermi surfaces.

which results in the compensation of the hole and electron carriers[47, 48]. Meanwhile, the nodal chain and nodal rings around the Fermi level make the hole and electron carriers have high mobility. According to the two-band model, CrB_4 has a large magnetoresistance effect when the applied electric and magnetic fields are perpendicular to each other. Due to the existence of type-II Dirac fermions, CrB_4 may have anisotropic negative magnetoresistance effect when the applied electric and magnetic fields are parallel[25, 26].

It is well known that nodal ring semimetals have topologically protected boundary states. CrB_4 has five nodal rings which can be projected onto the (001) and (010) surfaces (Fig. 2(c)). Therefore, CrB_4 has topologically protected boundary states on the both (001) and (010) surfaces. Then, we calculate the boundary states of CrB_4 on the (001) and (010) surfaces, which are shown in Fig. 3 and Fig. 4, respectively. For the (001) surface, CrB_4 has three topologically protected surface states crossing the Fermi levels deriving from the three nodal rings projected onto the (001) surface. More importantly, the Fermi arcs of CrB_4 at the Fermi level span the entire BZ. For the (010) surface, CrB_4 has two topologically protected surface states near the Fermi level deriving from two small nodal rings projected onto the (010) surface. Moreover, the Fermi arcs at the Fermi level also span the entire BZ. The Fermi arcs across the entire BZ at the Fermi level may result in CrB_4 having good catalytic property[5, 6].

When considering SOC, the symmetry of CrB_4 changes from D_{2h} point group to D_{2h} double point group. The highest symmetry for the high-symmetry axis in the BZ is C_{2v} double group, such as the Γ -X axis. Since there is only one two-dimensional irreducible representation for C_{2v} double group, both the nodal rings and nodal chain of CrB_4 must open an energy gap. Since both B and Cr

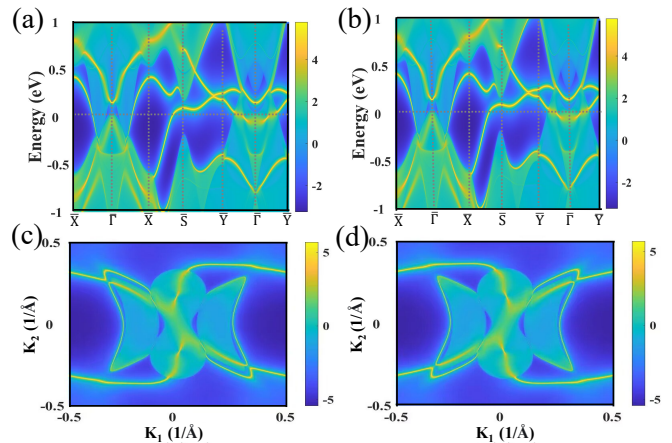


FIG. 3. Spectral function along the high-symmetry directions of CrB_4 left (a) and right (b) terminations for the (001) surface, which are contributed by Cr-B layers. The Fermi arcs at the Fermi level for left (c) and right (d) terminations.

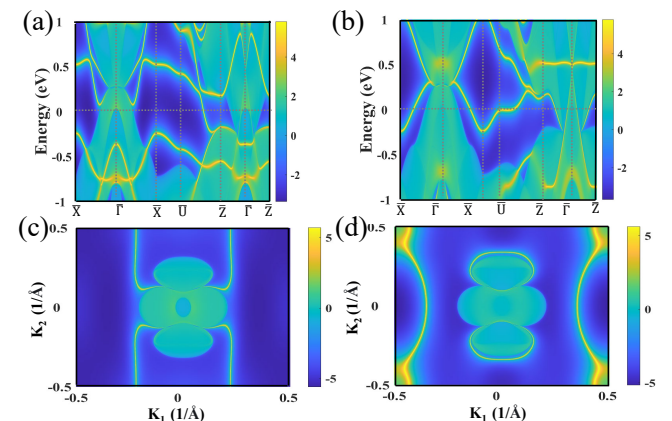


FIG. 4. Spectral function along the high-symmetry directions of CrB_4 left (a) and right (b) terminations for the (010) surface, which are contributed by B layers. The Fermi arcs at the Fermi level for left (c) and right (d) terminations.

atoms are light elements, the SOC effect of CrB_4 is very weak. With SOC(as shown in Fig.6), the sizes of the open bandgaps at the Γ -X and Γ -Y Dirac points are 2 meV, 27meV, and 18 meV respectively for CrB_4 (Fig. 5(a)). Considering that the SOC effect of the 2p orbitals of a B atom is much smaller than 1 meV, the four bands near the Fermi level are mainly contributed by the 3d orbitals of the Cr atom, which is also proved by the calculation of the DOS of CrB_4 (Fig. 2(a)). Due to the weak SOC effect, CrB_4 can be a model material for studying the novel physical properties of the type-II Dirac nodal chain in experiment.

On the other hand, what topological phase will CrB_4 transition from Dirac nodal chain semi-metal to under SOC? Since the parities of the two inversion bands at the time-reversal invariant Γ point are opposite (Fig. 5(a)), CrB_4 may be a strong topological insulator. In order

TABLE I. The product of parity of eight time-reversal-invariant points (TRIPs) for the 24 bands below the yellow band.

TRIPs	Γ	Z	U	R	T	X	Y	S	Total
parity	-	+	+	+	+	+	+	+	-

to determine the Z_2 topological invariants of CrB_4 , we need to calculate the parities of the eight time-reversal invariant points for 48 bands below the yellow bands[49].

$$(x, y, z) \xrightarrow{C_{2x}(\frac{1}{2}, \frac{1}{2}, \frac{1}{2})} (x + \frac{1}{2}, -y + \frac{1}{2}, -z + \frac{1}{2})$$

$$\xrightarrow{I} (-x - \frac{1}{2}, y - \frac{1}{2}, z - \frac{1}{2}) \quad (1)$$

$$(x, y, z) \xrightarrow{I} (-x, -y, -z)$$

$$\xrightarrow{C_{2x}(\frac{1}{2}, \frac{1}{2}, \frac{1}{2})} (-x + \frac{1}{2}, y + \frac{1}{2}, z + \frac{1}{2}) \quad (2)$$

In fact, the nonsymmorphic symmetry of CrB_4 can greatly simplify the calculation of Z_2 topological invariants. The SOC effect does not change the parity of time-reversal invariant points, thus we only need to perform symmetry analysis without SOC. According to equations (1) and (2), $C_{2x}(1/2, 1/2, 1/2)I = IC_{2x}(1/2, 1/2, 1/2)e^{-ikT}$, where T represents the translation (1,1,1). Obviously, the fractional translation (1/2, 1/2, 1/2) makes C_{2x} and I anticommutative at the time-reversal invariant X, Y, Z, and R points. Suppose Ψ is an eigenstate of I with eigenvalue to be 1. Since $C_{2x}(1/2, 1/2, 1/2)$ and I are anticommutative, $C_{2x}(1/2, 1/2, 1/2)\Psi$ is eigenstate of I with eigenvalue to be -1. Moreover, the Hamiltonian of CrB_4 commutes with $C_{2x}(1/2, 1/2, 1/2)$ and I, so Ψ and $C_{2x}(1/2, 1/2, 1/2)\Psi$ form a double degenerate state at time-reversal invariant X, Y, Z, and R points as shown in Fig. 2(a). Since the symmetry analysis is general, every band is of double degeneracy at the time-reversal invariant X, Y, Z, and R points, and the parity product of every doubly degenerate band is -1. There are 12 doubly degenerate bands below the yellow band, so the parity product of the occupying states at the time-reversal invariant points X, Y, Z and R is 1.

Similar to the time-reversal invariant X, Y, Z and R points, our analysis indicates the $C_{2x}(1/2, 1/2, 1/2)$ and M_z being anticommutative at the time-reversal invariant U and T points. If Ψ is the eigenstate of M_z with the eigenvalue 1, $C_{2x}(1/2, 1/2, 1/2)\Psi$ is the eigenstate of M_z with the eigenvalue -1. The Hamiltonian of CrB_4 is commutative with both $C_{2x}(1/2, 1/2, 1/2)$ and M_z , so Ψ and $C_{2x}(1/2, 1/2, 1/2)\Psi$ form a doubly degenerate state. Given that I is also commutative with both $C_{2x}(1/2, 1/2, 1/2)$ and M_z , Ψ and $C_{2x}(1/2, 1/2, 1/2)\Psi$ have the same parity. Since every band is of double degeneracy at the time-reversal invariant U, and T points, and the parity product of every doubly degenerate band is 1, so the product of the parity of the time-reversal invariant U and

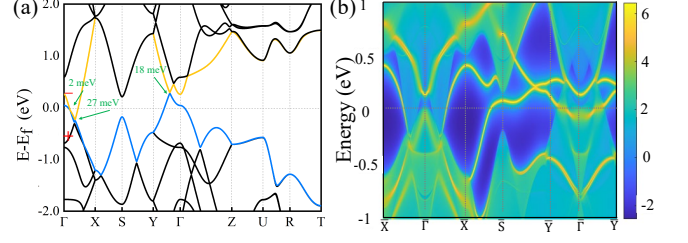


FIG. 5. (a) The band structure for CrB_4 with SOC along high-symmetry directions. (b) Spectral function along the high-symmetry directions left terminations for the (001) surface. The '+' and '-' represent parity for space-inversion symmetry.

T points is 1 for the 12 doubly degenerate bands below the yellow band.

For the time-reversal invariant S point, $(C_{2x}(1/2, 1/2, 1/2)T)^2$ is equal to -1, which causes Ψ and $C_{2x}(1/2, 1/2, 1/2)T\Psi$ to become Kramers degenerate. Since $C_{2x}(1/2, 1/2, 1/2)T$ and I are commutative, the product of parity of every degenerate state at the time-reversal invariant S point is 1. Correspondingly, the product of parity at the time-reversal invariant S point is also 1 for the 12 doubly degenerate bands below the yellow band. These results of the above symmetry analysis are shown in Table 1. Thus the Z_2 topological invariant of CrB_4 depends only on the parity of the Γ point. Our calculations show that the product of parity at the time-reversal invariant Γ point for the 24 non-degenerate bands below the yellow band is -1 (table I). When SOC is considered, the 24 bands below the yellow band become 48 bands. However, the calculation of the Z_2 topological invariants requires only the product of the parity of half of the 48 bands, which is consistent with the result of the parity product of the 24 bands without SOC. According to these results in Table I, the Z_2 topological invariants are (1,000) for CrB_4 , which is also consistent with calculations of WannierTools packages. Therefore, CrB_4 is a strong topological insulator.

The strong topological insulator has nontrivial Dirac surface states protected by the time-reversal symmetry. The calculated topological surface states of CrB_4 on the (001) surface are shown Fig. 5(b). Compared with Fig. 3(a), one topologically protected surface state splits into two, but the splits are very small, so the Dirac points of the surface state protected by the time-reversal symmetry are not obvious, which also implies the weak SOC effect of CrB_4 . Since there are only two non-trivial bands around the Fermi level and its topologically protected surface states at the Fermi level span the entire BZ, CrB_4 is an ideal type-II Dirac nodal chain semimetal with distinct properties.

IV. IN SUMMARY

Based on symmetry analysis and the first-principles electronic structure calculations, we predict that CrB_4 is a topological semimetal with a type-II nodal chain and two nodal rings protected respectively by mirror symmetry and IT symmetry. More importantly, the topologically protected drumhead surface states of CrB_4 span the entire BZ at the Fermi level. Meanwhile, there are only two nontrivial bands crossing the Fermi level, thus CrB_4 is an ideal type-II Dirac nodal chain semimetal with distinct properties. When considering SOC, CrB_4 transforms from topological semimetal phase to topological insulator phase. Because it has been synthesized experimentally and has a very weak SOC effect, CrB_4 is an ideal material platform for studying the exotic properties

of type-II Dirac nodal chain semimetals in experiment.

ACKNOWLEDGMENTS

This work was financially supported by the National Natural Science Foundation of China (Grant No.11934020, No.12204533, No.62476278, No.62206299), the Fundamental Research Funds for the Central Universities, and the Research Funds of Renmin University of China (Grant No. 24XNKJ15) and the Innovation Program for Quantum Science and Technology (Grant No. 2021ZD0302402). Computational resources have been provided by the Physical Laboratory of High Performance Computing at Renmin University of China.

-
- [1] H. Weng, X. Dai, and Z. Fang, Topological semimetals predicted from first-principles calculations, *J. Phys. Condens. Matter* **28**, 303001 (2016).
- [2] A. Bernevig, H. Weng, Z. Fang, and X. Dai, Recent progress in the study of topological semimetals, *J. Phys. Soc. Jpn.* **87**, 041001 (2018).
- [3] G. X. Jinyu Zou, Zhuoran He, The study of magnetic topological semimetals by first principles calculations, *npj Comput. Mater.* **5**, 96 (2019).
- [4] B. Q. Lv, T. Qian, and H. Ding, Experimental perspective on Three-dimensional topological semimetals, *Rev. Mod. Phys.* **93**, 025002 (2021).
- [5] G. Li and C. Felser, Heterogeneous catalysis at the surface of topological materials, *Appl. Phys. Lett.* **116**, 070501 (2020).
- [6] R. Xie, T. Zhang, H. Weng, and G.-L. Chai, Progress, advantages, and challenges of topological material catalysts, *Small. Sci.* **2**, 2100106 (2022).
- [7] X. Wan, A. M. Turner, A. Vishwanath, and S. Y. Savrasov, Topological semimetal and Fermi-arc surface states in the electronic structure of pyrochlore iridates, *Phys. Rev. B* **83**, 205101 (2011).
- [8] H. Weng, C. Fang, Z. Fang, B. A. Bernevig, and X. Dai, Weyl semimetal phase in noncentrosymmetric transition-metal monophosphides, *Phys. Rev. X* **5**, 011029 (2015).
- [9] S. M. Young, S. Zaheer, J. C. Y. Teo, C. L. Kane, E. J. Mele, and A. M. Rappe, Dirac semimetal in Three dimensions, *Phys. Rev. Lett.* **108**, 140405 (2012).
- [10] Z. Wang, Y. Sun, X.-Q. Chen, C. Franchini, G. Xu, H. Weng, X. Dai, and Z. Fang, Dirac semimetal and topological phase transitions in A_3Bi ($\text{A}=\text{Na}, \text{K}, \text{Rb}$), *Phys. Rev. B* **85**, 195320 (2012).
- [11] Z. Wang, H. Weng, Q. Wu, X. Dai, and Z. Fang, Three-dimensional Dirac semimetal and quantum transport in Cd_3As_2 , *Phys. Rev. B* **88**, 125427 (2013).
- [12] Z. K. Liu, B. Zhou, Y. Zhang, Z. J. Wang, H. M. Weng, D. Prabhakaran, S.-K. Mo, Z. X. Shen, Z. Fang, X. Dai, Z. Hussain, and Y. L. Chen, Discovery of a Three-dimensional topological Dirac semimetal, Na_3Bi , *Science* **343**, 864 (2014).
- [13] B. Bradlyn, J. Cano, Z. Wang, M. G. Vergniory, C. Felser, R. J. Cava, and B. A. Bernevig, Beyond Dirac and Weyl fermions: Unconventional quasiparticles in conventional crystals, *Science* **353**, aaf5037 (2016).
- [14] H. Weng, C. Fang, Z. Fang, and X. Dai, Topological semimetals with triply degenerate nodal points in θ -phase tantalum nitride, *Phys. Rev. B* **93**, 241202 (2016).
- [15] Z. Zhu, G. W. Winkler, Q. Wu, J. Li, and A. A. Soluyanov, Triple point Topological metals, *Phys. Rev. X* **6**, 031003 (2016).
- [16] P.-J. Guo, H.-C. Yang, K. Liu, and Z.-Y. Lu, Triply degenerate nodal points in $\text{R Rh}_6\text{Ge}_4$ ($\text{R}=\text{Y}, \text{La}, \text{Lu}$), *Phys. Rev. B* **98**, 045134 (2018).
- [17] N. Kumar, M. Yao, J. Nayak, M. G. Vergniory, J. Bannies, Z. Wang, N. B. M. Schröter, V. N. Strocov, L. Müchler, W. Shi, E. D. L. Rienks, J. L. Mañes, C. Shekhar, S. S. P. Parkin, J. Fink, G. H. Fecher, Y. Sun, B. A. Bernevig, and C. Felser, Signatures of sixfold degenerate exotic fermions in a superconducting metal PdSb_2 , *Adv. Mater.* **32**, 1906046 (2020).
- [18] X. Yang, T. A. Cochran, R. Chapai, D. Tristant, J.-X. Yin, I. Belopolski, Z. b. u. b. a. Chéng, D. Multer, S. S. Zhang, N. Shumiya, M. Litskevich, Y. Jiang, G. Chang, Q. Zhang, I. Vekhter, W. A. Shelton, R. Jin, S.-Y. Xu, and M. Z. Hasan, Observation of sixfold degenerate fermions in PdSb_2 , *Phys. Rev. B* **101**, 201105 (2020).
- [19] B. J. Wieder, Y. Kim, A. M. Rappe, and C. L. Kane, Double Dirac semimetals in Three-dimensions, *Phys. Rev. Lett.* **116**, 186402 (2016).
- [20] P.-J. Guo, Y.-W. Wei, K. Liu, Z.-X. Liu, and Z.-Y. Lu, Eightfold degenerate fermions in Two-dimensions, *Phys. Rev. Lett.* **127**, 176401 (2021).
- [21] A. A. Burkov, M. D. Hook, and L. Balents, Topological nodal semimetals, *Phys. Rev. B* **84**, 235126 (2011).
- [22] H. Weng, Y. Liang, Q. Xu, R. Yu, Z. Fang, X. Dai, and Y. Kawazoe, Topological node-line semimetal in three-dimensional graphene networks, *Phys. Rev. B* **92**, 045108 (2015).
- [23] R. Yu, H. Weng, Z. Fang, X. Dai, and X. Hu, Topological Node-Line Semimetal and Dirac Semimetal State in Antiperovskite Cu_3PdN , *Phys. Rev. Lett.* **115**, 036807 (2015).

- [24] W. Wu, Y. Liu, S. Li, C. Zhong, Z.-M. Yu, X.-L. Sheng, Y. X. Zhao, and S. A. Yang, Nodal surface semimetals: Theory and material realization, *Phys. Rev. B* **97**, 115125 (2018).
- [25] A. A. Soluyanov, D. Gresch, Z. Wang, Q. Wu, M. Troyer, X. Dai, and B. A. Bernevig, Type-II Weyl semimetals, *Nature* **527**, 495 (2015).
- [26] H. Huang, S. Zhou, and W. Duan, Type-II Dirac fermions in the PtSe₂ class of transition metal dichalcogenides, *Phys. Rev. B* **94**, 121117 (2016).
- [27] P.-J. Guo, H.-C. Yang, K. Liu, and Z.-Y. Lu, Type-II Dirac semimetals in the YPd₂Sn class, *Phys. Rev. B* **95**, 155112 (2017).
- [28] T. Bzdusek, Q. Wu, A. Ruegg, M. Sigrist, and A. A. Soluyanov, Nodal-chain metals, *Nature* **538**, 75 (2016).
- [29] M. Ezawa, Topological semimetals carrying arbitrary Hopf numbers: Fermi surface topologies of a Hopf link, Solomon's knot, trefoil knot, and other linked nodal varieties, *Phys. Rev. B* **96**, 041202 (2017).
- [30] Z. Liu, R. Lou, P. Guo, Q. Wang, S. Sun, C. Li, S. Thirupathiah, A. Fedorov, D. Shen, K. Liu, H. Lei, and S. Wang, Experimental observation of Dirac nodal links in centrosymmetric semimetal TiB₂, *Phys. Rev. X* **8**, 031044 (2018).
- [31] R. Lou, P. Guo, M. Li, Q. Wang, Z. Liu, S. Sun, C. Li, X. Wu, Z. Wang, Z. Sun, D. Shen, Y. Huang, K. Liu, Z.-Y. Lu, H. Lei, H. Ding, and S. Wang, Experimental observation of bulk nodal lines and electronic surface states in ZrB₂, *npj Quantum Mater.* **3**, 43 (2018).
- [32] Q. Yan, R. Liu, Z. Yan, B. Liu, H. Chen, Z. Wang, and L. Lu, Experimental discovery of nodal chains, *Nat. Phys.* **14**, 461 (2018).
- [33] Zhao, M. and Zhuang, Z.-Y. and Wu, F. and Leng, P. and Joseph, N. B. and Xie, X. and Ozerov, M. and He, S. and Chen, Y. and Narayan, A. and Liu, Z. and Xiu, and Faxian, Observation of type-II topological nodal-line fermions in ZrSiSe, *ACS Nano.* , 16684 (2024).
- [34] W. Kohn and L. J. Sham, Self-consistent equations including exchange and correlation effects, *Phys. Rev.* **140**, A1133 (1965).
- [35] P. Hohenberg and W. Kohn, Inhomogeneous electron gas, *Phys. Rev.* **136**, B864 (1964).
- [36] G. Kresse and J. Furthmüller, Efficient iterative schemes for ab initio total-energy calculations using a plane-wave basis set, *Phys. Rev. B* **54**, 11169 (1996).
- [37] G. Kresse and J. Hafner, Ab initio molecular dynamics for liquid metals, *Phys. Rev. B* **47**, 558 (1993).
- [38] G. Kresse and J. Furthmüller, Efficiency of ab-initio total energy calculations for metals and semiconductors using a plane-wave basis set, *Comput. Mater. Sci.* **6**, 15 (1996).
- [39] G. Kresse and D. Joubert, From ultrasoft pseudopotentials to the projector augmented-wave method, *Phys. Rev. B* **59**, 1758 (1999).
- [40] J. P. Perdew, K. Burke, and M. Ernzerhof, Generalized gradient approximation made simple, *Phys. Rev. Lett.* **77**, 3865 (1996).
- [41] N. Marzari, A. A. Mostofi, J. R. Yates, I. Souza, and D. Vanderbilt, Maximally localized wannier functions: Theory and applications, *Rev. Mod. Phys.* **84**, 1419 (2012).
- [42] A. A. Mostofi, J. R. Yates, G. Pizzi, Y.-S. Lee, I. Souza, D. Vanderbilt, and N. Marzari, An updated version of wannier90: A tool for obtaining maximally-localised wannier functions, *Comput. Phys. Commun.* **185**, 2309 (2014).
- [43] G. Pizzi, V. Vitale, R. Arita, S. Blügel, F. Freimuth, G. Géranton, M. Gibertini, D. Gresch, C. Johnson, T. Koretsune, J. Ibañez-Azpiroz, H. Lee, J.-M. Lihm, D. Marchand, A. Marrazzo, Y. Mokrousov, J. I. Mustafa, Y. Nohara, Y. Nomura, L. Paulatto, S. Poncé, T. Ponweiser, J. Qiao, F. Thöle, S. S. Tsirkin, M. Wierzbowska, N. Marzari, D. Vanderbilt, I. Souza, A. A. Mostofi, and J. R. Yates, Wannier90 as a community code: new features and applications, *J. Phys.: Condens. Matter* **32**, 165902 (2020).
- [44] Q. Wu, S. Zhang, H.-F. Song, M. Troyer, and A. A. Soluyanov, Wanniertools: An open-source software package for novel topological materials, *Comput. Phys. Commun.* **224**, 405 (2018).
- [45] A. Knappschneider, C. Litterscheid, D. Dzivenko, J. A. Kurzman, R. Seshadri, N. Wagner, J. Beck, R. Riedel, and B. Albert, Possible superhardness of CrB₄, *Inorg. Chem.* **52**, 540 (2013).
- [46] H. Niu, J. Wang, X.-Q. Chen, D. Li, Y. Li, P. Lazar, R. Podlucky, and A. N. Kolmogorov, Structure, bonding, and possible superhardness of CrB₄, *Phys. Rev. B* **85**, 144116 (2012).
- [47] P.-J. Guo, H.-C. Yang, B.-J. Zhang, K. Liu, and Z.-Y. Lu, Charge compensation in extremely large magnetoresistance materials LaSb and LaBi revealed by first-principles calculations, *Phys. Rev. B* **93**, 235142 (2016).
- [48] M. N. Ali, J. Xiong, S. Flynn, J. Tao, Q. D. Gibson, L. M. Schoop, T. Liang, N. Haldolaarachchige, M. Hirschberger, N. P. Ong, and R. J. Cava, Large, non-saturating magnetoresistance in WTe₂, *Nature* **514**, 205 (2014).
- [49] L. Fu, C. L. Kane, and E. J. Mele, Topological insulators in Three-dimensions, *Phys. Rev. Lett.* **98**, 106803 (2007).
- [50] D. Takane, Z. Wang, S. Souma, K. Nakayama, C. X. Trang, T. Sato, T. Takahashi, and Y. Ando, Dirac-node arc in the topological line-node semimetal HfSiS, *Phys. Rev. B* **94**, 121108 (2016).
- [51] Q. Xu, R. Yu, Z. Fang, X. Dai, and H. Weng, Topological nodal line semimetals in the CaP₃ family of materials, *Phys. Rev. B* **95**, 045136 (2017).